INTERNATIONAL JOURNAL FOR NUMERICAL METHODS IN FLUIDS, VOL. 19, 667–685 (1994)

A CHARACTERISTIC-BASED METHOD FOR INCOMPRESSIBLE FLOWS

D. DRIKAKIS

Lehrstuhl für Strömungsmechanik, Universität Erlangen-Nürnberg, Cauerstr. 4, W-91058 Erlangen, Germany

AND

P. A. GOVATSOS AND D. E. PAPANTONIS*

National Technical University of Athens, Department of Mechanical Engineering, Laboratory of Hydraulic Turbomachines, PO Box 64070, 15710 Zografos Athens, Greece

SUMMARY

A new characteristic-based method for the solution of the 2D laminar incompressible Navier–Stokes equations is presented. For coupling the continuity and momentum equations, the artificial compressibility formulation is employed. The primitives variables (pressure and velocity components) are defined as functions of their values on the characteristics. The primitives variables on the characteristics are calculated by an upwind differencing scheme based on the sign of the local eigenvalue of the Jacobian matrix of the convective fluxes. The upwind scheme uses interpolation formulae of third-order accuracy. The time discretization is obtained by the explicit Runge–Kutta method. Validation of the characteristic-based method is performed on two different cases: the flow in a simple cascade and the flow over a backward-facing step.

KEY WORDS Incompressible flows Navier–Stokes equations Riemann solver Artificial compressibility

1. INTRODUCTION

The development of solution methodologies for the unsteady incompressible Navier–Stokes equations has received considerable attention in the past. The solution of incompressible flows in primitive variables involves the difficulty of coupling the changes in the velocity field with the changes in the pressure field while at the same time satisfying the continuity. For two-dimensional flows the streamfunction–vorticity formulation can be used as an alternative, but this is less effective in three dimensions and other methods have to be used. Most methods using primitive variables can be classified into two broad categories.

The first of these is the pressure Poisson method first introduced by Harlow and Welch.[1] In this method a Poisson equation or a specially formulated 'correction' equation which is formed from the momentum equations is solved for the pressure at each iteration such that the continuity equation will be satisfied at the next iteration.[1–3] In this procedure the momentum equations are used for the velocity field. The second category is that of artificial compressibility. This method was first introduced by Chorin[4] in obtaining steady state solutions. In the artificial compressibility (or pseudocompressibility) formulation a time derivative of the pressure is added to the continuity equation and therefore a coupling of the pressure and velocity is obtained.

* Author to whom correspondence should be addressed.

CCC 0271-2091/94/200667-19

Received November 1993
Revised April 1994

During recent years several authors have used the artifical compressibility formulation in computing steady and unsteady incompressible flows.[5–14]

The artificial compressibility formulation transforms the incompressible Euler equations to a totally hyperbolic system, and therefore numerical methods which have initially been developed for the compressible Euler and Navier–Stokes can be extended to incompressible flows. In the past flux-difference-splitting methods for incompressible flows have been developed by Hartwich *et al.*,[11] Rogers and Kwak[12,13] and Kwak *et al.*[9] Merkle and Athavale[10] have also developed an upwind differencing method for unsteady incompressible flows, while Dick and Linden[14] have developed flux difference splitting for the steady incompressible equations. Furthermore, prediction of incompressible flows by the approximate factorization technique has also been presented.[15] Besides the above categories, the penalty method,[16] which has mainly been used in the finite element community, has to be reported. In this method a pressure term instead of a time derivative of pressure is added to the continuity equation. A combination of the penalty and pseudocompressibility methods for solving the Navier–Stokes equations has also been proposed.[17]

The objective of this work is to present a characteristic-based method which exploits the hyperbolic properties of the incompressible inviscid equations as they are introduced in the artificial compressibility formulation. In the past Eberle[18] has developed a characteristic flux-averaging scheme for an ideal gas and this method has since been reformulated for real gas problems by other authors.[19,20] In the present work a new characteristic-based method is developed for the incompressible Navier–Stokes equations. The motivation for the present work originates from previous experience of successful implementation of characteristic flux averaging in compressible flows.

The present method defines the primitives variables as functions of their corresponding values on the characteristics. Consequently, the values on the characteristics are calculated by an upwind differencing scheme based on the sign of the local eigenvalue of the Jacobian matrix of the convective fluxes. The Navier–Stokes terms are discretized by an 'upwind'-type scheme,[21] while the time integration is obtained by a multistage Runge–Kutta scheme.[22,23] Validation of the Navier–Stokes solver is presented for the separated laminar flow in a cascade of circular aerofoils and for the flow over a backward-facing step, where experimental results were available.

2. GOVERNING EQUATIONS AND ARTIFICIAL COMPRESSIBILITY

The unsteady flow of an incompressible fluid is governed by the Navier–Stokes equations written in tensor notation as

$$\frac{\partial u_i}{\partial x_i} = 0, \tag{1a}$$

$$\frac{\partial u_i}{\partial t} + \frac{\partial u_i u_j}{\partial x_j} = -\frac{\partial p}{\partial x_i} + \frac{\partial \tau_{ij}}{\partial x_j}, \tag{1b}$$

where t is time, $x_i (i = 1,2)$ are Cartesian co-ordinates, u_i are the corresponding velocity components, p is the pressure and τ_{ij} is the viscous stress tensor.

The above system of equations can be modified by introducing the artificial compressibility concept[4] through a time derivative of pressure in the continuity equation (1a):

$$\frac{1}{\beta}\frac{\partial p}{\partial t} + \frac{\partial u_i}{\partial x_i} = 0. \tag{2}$$

For incompressible flows equations (2) and (1b) can be considered using as primitive variables the pressure and velocity components. The parameter β is the artificial compressibility and is to be chosen to ensure the fastest convergence to the steady state. If a transient solution were desired, β would have to be chosen large. In the present work steady state solutions are considered and therefore the value of β has to be selected to enhance convergence.

The Navier–Stokes equations with the artificial compressibility term added can be expressed in generalized co-ordinates $\xi = \xi(x, z)$ and $\zeta = \zeta(x, z)$ and dimensionless form by the vector system

$$\frac{\partial(JU)}{\partial t} + \frac{\partial E_{\text{inv}}}{\partial \xi} + \frac{\partial G_{\text{inv}}}{\partial \zeta} = \frac{1}{Re}\left(\frac{\partial E_{\text{vis}}}{\partial \xi} + \frac{\partial G_{\text{vis}}}{\partial \zeta}\right), \tag{3}$$

where Re is the Reynolds number and U is the unknown solution vector

$$U = (p/\beta, u, w)^{\mathrm{T}}. \tag{4}$$

The inviscid flux vectors E_{inv} and G_{inv} and the viscous ones E_{vis} and G_{vis} can be written by superposition of the Cartesian inviscid ($\tilde{E}$, $\tilde{G}$) and viscous ($\tilde{R}$, $\tilde{S}$) fluxes respectively as

$$E_{\text{inv}} = J(\tilde{E}\xi_x + \tilde{G}\xi_z), \tag{5a}$$

$$G_{\text{inv}} = J(\tilde{E}\zeta_x + \tilde{G}\zeta_z), \tag{5b}$$

$$E_{\text{vis}} = J(\tilde{R}\xi_x + \tilde{S}\xi_z), \tag{5c}$$

$$G_{\text{vis}} = J(\tilde{R}\zeta_x + \tilde{S}\zeta_z), \tag{5d}$$

where

$$\tilde{E} = (u, u^2 + p, uw)^{\mathrm{T}}, \tag{6a}$$

$$\tilde{G} = (w, uw, w^2 + p)^{\mathrm{T}}, \tag{6b}$$

$$\tilde{R} = (0, \tau_{xx}, \tau_{xz})^{\mathrm{T}}, \tag{6c}$$

$$\tilde{S} = (0, \tau_{zx}, \tau_{zz})^{\mathrm{T}}. \tag{6d}$$

The indices x and z denote partial derivatives, except for the stresses τ_{xx}, τ_{xz}, and τ_{zz}. The stresses are defined as

$$\tau_{xx} = -\tfrac{2}{3}(-2u_x + w_z), \tag{7a}$$

$$\tau_{xz} = \tau_{zx} = (w_x + u_z), \tag{7b}$$

$$\tau_{zz} = -\tfrac{2}{3}(u_x - 2w_z). \tag{7c}$$

Finally, u and w are the velocity components in the directions x and z respectively and $J = x_\xi z_\zeta - x_\zeta z_\xi$ is the Jacobian of the transformation $\xi = \xi(x, z)$, $\zeta = \zeta(x, z)$ from Cartesian to generalized co-ordinates.

3. CHARACTERISTIC-BASED METHOD

Neglecting the viscous terms from the Navier–Stokes equations (3), the incompressible Euler equations are obtained as

$$\frac{\partial(JU)}{\partial t} + \frac{\partial E_{\text{inv}}}{\partial \xi} + \frac{\partial G_{\text{inv}}}{\partial \zeta} = 0. \tag{8}$$

The objective of the present work is to develop a numerical method which exploits the hyperbolic properties of the above system of equations. For this purpose a characteristic-based method (or a local Riemann solver) will be examined in the next paragraphs. This method is used for the discretization of the convective part of the Navier–Stokes equations.

The Euler equations can be written in discretized form using a finite volume scheme. All quantities are considered to be located at the centre of the corresponding cell. In two dimensions this can be done by considering a volume (i, k) (Figure 1) with cell faces $(i + \frac{1}{2}, k)$ and $(i - \frac{1}{2}, k)$ in the ξ-direction and $(i, k + \frac{1}{2})$ and $(i, k - \frac{1}{2})$ in the ζ-direction.

Using the finite volume concept, the Euler equations are written as

$$\frac{\partial(JU)}{\partial t} + E_{i+1/2,k} - E_{i-1/2,k} + G_{i,k+1/2} - G_{i,k-1/2} = 0. \tag{9}$$

In order to analyse the Euler equations, a simpler form than equation (8) can be chosen. This can be done by splitting the Euler equations into two one-dimensional equations

$$\frac{\partial(JU)}{\partial t} + \frac{\partial E_{\text{inv}}}{\partial \xi} = 0 \tag{10a}$$

and

$$\frac{\partial(JU)}{\partial t} + \frac{\partial G_{\text{inv}}}{\partial \zeta} = 0. \tag{10b}$$

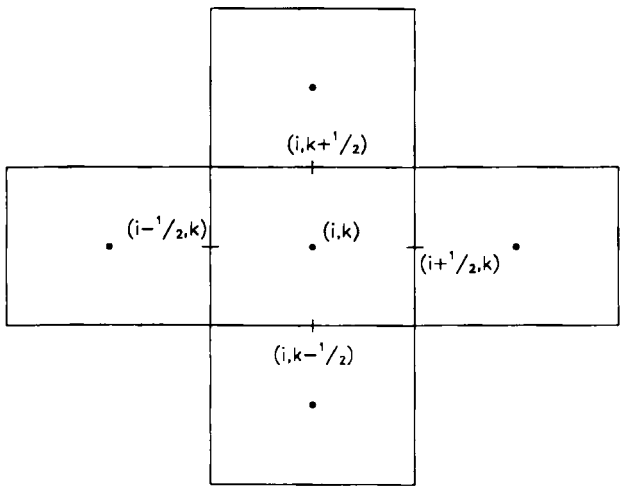

Figure 1. A finite volume (i, k) with its cell faces

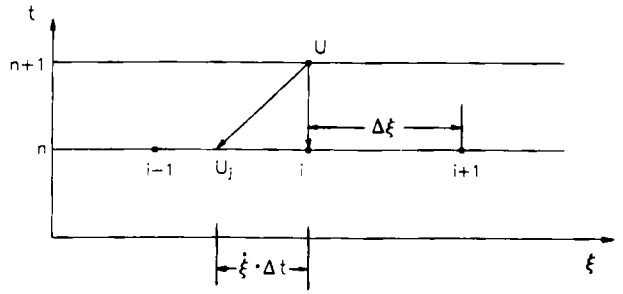

Figure 2. Schematic representation of the characteristic scheme

We will present the analysis of the method for equation (10a). This equation can be used for the development of the local Riemann solution in the ξ-direction. Similarly equation (10b) can be analysed, resulting in a local Riemann solution in the ζ-direction.

The non-conservative form of equation (10a) is

$$\frac{J}{\beta} p_t + u_\xi \xi_x + w_\xi \xi_z = 0, \tag{11a}$$

$$Ju_t + u_\xi(u\xi_x + w\xi_z) + u(u_\xi \xi_x + w_\xi \xi_z) + p_\xi \xi_x = 0, \tag{11b}$$

$$Jw_t + w_\xi(u\xi_x + w\xi_z) + w(u_\xi \xi_x + w_\xi \xi_z) + p_\xi \xi_z = 0, \tag{11c}$$

In the last system of equations the space derivatives are usually calculated by the initial data at time level n. In order to obtain time integration of equations (11), the update values of the vector $U = (p/\beta, u, w)^T$ at time level $n + 1$ can be defined by a linear Taylor series expansion around the known previous time level (Figure 2).

A backward Taylor series expansion can be such that the vector U is to be defined as a function of the U_j-values which are inside the limits of a stable integration.[24] This leads to the definition

$$U = U_j + \Delta\tilde{\xi} U_\xi + \dot{U}\Delta t \quad \text{or} \quad \dot{U} = \frac{U - U_j}{\Delta t} - U_\xi \frac{\Delta\tilde{\xi}}{\Delta t}, \tag{12}$$

where $(\cdot) = \partial/\partial t$. The interval $\Delta\tilde{\xi}$ can be defined by introducing a wave speed $\dot{\xi}$ such that

$$\Delta\tilde{\xi} = \dot{\xi}\Delta t$$

and subsequently the line with the slope $1/\dot{\xi}$ is the characteristic.

If we consider a dimensional analysis, we find that the term $\dot{\xi}$ is not really a physical speed, because ξ is dimensionless and therefore $\dot{\xi}$ is an inverse time. Following Reference 24, in order to enter a physical wave speed with a proper dimension, the wave speed λ is introduced via

$$\dot{\xi} = \lambda \frac{\sqrt{(\xi_x^2 + \xi_z^2)}}{J}.$$

Therefore equation (12) yields

$$\dot{U} = \frac{U - U_j}{\Delta t} - U_\xi \lambda \frac{\sqrt{(\xi_x^2 + \xi_z^2)}}{J}. \tag{13}$$

By substitution of equation (13) into equations (11) the following equations are obtained:

$$\frac{1}{\beta}\frac{J}{\sqrt{(\xi_x^2+\xi_z^2)}\Delta t}(p-p_j)-\frac{1}{\beta}p_\xi\lambda+u_\xi\tilde{x}+w_\xi\tilde{z}=0, \tag{14a}$$

$$\frac{J}{\sqrt{(\xi_x^2+\xi_z^2)}\Delta t}(u-u_j)+u_\xi(\lambda_0-\lambda)+u(u_\xi\tilde{x}+w_\xi\tilde{z})+p_\xi\tilde{x}=0, \tag{14b}$$

$$\frac{J}{\sqrt{(\xi_x^2+\xi_z^2)}\Delta t}(w-w_j)+w_\xi(\lambda_0-\lambda)+w(u_\xi\tilde{x}+w_\xi\tilde{z})+p_\xi\tilde{z}=0, \tag{14c}$$

where

$$\lambda_0=u\tilde{x}+w\tilde{z},\qquad \tilde{x}=\frac{\xi_x}{\sqrt{(\xi_x^2+\xi_x^2)}},\qquad \tilde{z}=\frac{\xi_z}{\sqrt{(\xi_x^2+\xi_z^2)}}.$$

The spatial derivatives of u_ξ, w_ξ, and p_ξ can be eliminated from the above three equations following the method of Riemann.[25] Similar consideration has also been given by Eberle[24] for the compressible Euler equations. This consideration is the following. Because at each time the system of equations is zero, it can be multiplied by an arbitrary coefficient, and after the summation of the three equations the resulting equation will also be zero. This procedure yields the equation

$$\frac{J}{\Delta t\sqrt{(\xi_x^2+\xi_z^2)}}\left(\frac{a}{\beta}(p-p_j)+b(u-u_j)+c(w-w_j)\right)+p_\xi\left(-\frac{a}{\beta}\lambda+b\tilde{x}+c\tilde{z}\right)$$
$$+u_\xi[a\tilde{x}+b(\lambda_0-\lambda+u\tilde{x})+cw\tilde{x}]+w_\xi[a\tilde{z}+bu\tilde{z}+c(\lambda_0-\lambda+w\tilde{z})]=0, \tag{15}$$

where a, b and c are the coefficients that multiply equations (14a), (14b) and (14c) respectively. If we define the coefficients of the partial space derivatives to be zero, an ordinary difference equation will be obtained:

$$\frac{a}{\beta}(p-p_j)+b(u-u_j)+c(w-w_j)=0, \tag{16}$$

with

$$-a\frac{\lambda}{\beta}+b\tilde{x}+c\tilde{z}=0, \tag{17a}$$

$$a\tilde{x}+b(\lambda_0-\lambda+u\tilde{x})+cw\tilde{x}=0, \tag{17b}$$

$$a\tilde{z}+bu\tilde{z}+c(\lambda_0-\lambda+w\tilde{z})=0. \tag{17c}$$

By solving the last three equations, the coefficients a, b and c can be determined. A non-trivial solution is defined for each of the eigenvalues of the above system:

$$\lambda_0=u\tilde{x}+w\tilde{z}, \tag{18a}$$

$$\lambda_1=\lambda_0+\sqrt{(\lambda_0^2+\beta)}, \tag{18b}$$

$$\lambda_2=\lambda_0-\sqrt{(\lambda_0^2+\beta)}. \tag{18c}$$

For $\lambda = \lambda_0$ equations (17) give

$$a = \frac{b\tilde{x} + c\tilde{z}}{\lambda_0}\beta.$$

By substitution of the last equation into equation (16) we find

$$b[\tilde{x}(p - p_0) + \lambda_0(u - u_0)] + c[\tilde{z}(p - p_0) + \lambda_0(w - w_0)] = 0,$$

where the subscript '0' denotes that this equation corresponds to the zeroth eigenvalue. The last equation must be satisfied regardless of the values of the coefficients b and c. Therefore the terms in square brackets must be zero and the following equation is obtained:

$$(u - u_0)\tilde{z} - (w - w_0)\tilde{x} = 0. \tag{19}$$

Similarly for the eigenvalues λ_1 and λ_2 the following equations are obtained:

$$(p - p_1) + \lambda_1[\tilde{x}(u - u_1) + \tilde{z}(w - w_1)] = 0, \tag{20}$$

$$(p - p_2) + \lambda_2[\tilde{x}(u - u_2) + \tilde{z}(w - w_2)] = 0. \tag{21}$$

The values p_j, u_j and w_j with $j = 0, 1, 2$ are the values of the primitive variables on the three characteristics. Equations (19)–(21) are the three characteristic equations (or Riemann invariants). The solution of these equations gives the primitive variables p, u and w as functions of their characteristic values:

$$u = \tilde{x}R + \tilde{z}(u_0\tilde{z} - w_0\tilde{x}), \tag{22a}$$

$$w = \tilde{z}R - \tilde{x}(u_0\tilde{z} - w_0\tilde{x}), \tag{22b}$$

$$p = \frac{1}{2\sqrt{(\lambda_0^2 + \beta)}}(\lambda_1 k_2 - \lambda_2 k_1), \tag{22c}$$

where

$$R = \frac{1}{2\sqrt{(\lambda_0^2 + \beta)}}[(p_1 - p_2) + \tilde{x}(\lambda_1 u_1 - \lambda_2 u_2) + \tilde{z}(\lambda_1 w_1 - \lambda_2 w_2)], \tag{23a}$$

$$k_1 = p_1 + \lambda_1(u_1\tilde{x} + w_1\tilde{z}), \tag{23b}$$

$$k_2 = p_2 + \lambda_2(u_2\tilde{x} + w_2\tilde{z}). \tag{23c}$$

For the calculation of the inviscid flux E_{inv} on the cell face of the computational volume the values of the pressure and velocities from equations (22) are used.

The characteristic values p_j, u_j and w_j with $j = 0, 1, 2$ are defined by upwind differencing from the left or the right side of the cell face according to the sign of the eigenvalues:

$$U^j_{i+1/2} = \tfrac{1}{2}[(1 + \text{sign } \lambda_j)U^- + (1 - \text{sign } \lambda_j)U^+], \tag{24}$$

where $U^j_{i+1/2}$ is a vector containing the characteristic values for each $j = 0, 1, 2$. U^- and U^+ are the values of the characteristics variables from the left and the right side of the control volume respectively.

In order to increase the accuracy of the scheme, a third-order interpolation formula is employed according to Reference 19:

$$(U_{i+1/2})^- = \tfrac{1}{6}(5U_i - U_{i-1} + 2U_{i+1}), \tag{25a}$$

$$(U_{i+1/2})^+ = \tfrac{1}{6}(5U_{i+1} - U_{i+2} + 2U_i). \tag{25b}$$

These interpolation formulae have also been used in the past for the solution of the compressible Euler and Navier–Stokes equations, providing satisfactory accuracy and convergence properties.[19]

The analysis of the method was shown in this section for the inviscid flux E_{inv}. The construction of the characteristic-based method for the flux G_{inv} can be obtained in a similar way.

The solution of the Navier–Stokes equations requires also the discretization of the viscous terms. For this purpose an 'upwind'-type scheme for the cross-derivatives of the viscous fluxes and central discretization for the second-order derivatives were adopted.[21,26] The same scheme has been used successfully in the past for subsonic and supersonic flows.

4. TIME INTEGRATION OF THE INCOMPRESSIBLE EQUATIONS

For the time integration of the Navier–Stokes equations the explicit fourth-order Runge–Kutta time-stepping method was employed. The Runge–Kutta time-stepping method[22,23] can be written as

$$\begin{aligned} U^{(1)} &= U^n, \\ U^{(2)} &= U^{(1)} - \frac{\Delta t}{2} R(U)^{(1)}, \\ U^{(3)} &= U^{(2)} - \frac{\Delta t}{2} R(U)^{(2)}, \\ U^{(4)} &= U^{(3)} - \frac{\Delta t}{2} R(U)^{(3)}, \\ U^{n+1} &= U^n - \frac{\Delta t}{6}[R(U)^{(1)} + 2R(U)^{(2)} + 2R(U)^{(3)} + R(U)^{(4)}], \end{aligned} \tag{26}$$

where

$$R(U)^{(v)} = (E_{\text{inv}}^{(v)})_\xi + (G_{\text{inv}}^{(v)})_\zeta + (E_{\text{vis}}^{(v)})_\xi + (G_{\text{vis}}^{(v)})_\zeta.$$

For faster convergence to the steady state solution a local time stepping Δt is used:

$$\Delta t = \frac{\text{CFL}}{\max(\lambda_j)}, \quad j = 0, 1, 2,$$

where CFL is the Courant–Friedrichs–Lewy number. The bound values of CFL are discussed in the numerical calculation of the next section.

5. VALIDATION OF THE NAVIER–STOKES ALGORITHM

5.1. Flow in a cascade of circular aerofoils

The presented numerical method is first applied to the case of the steady state flow in a cascade formed by circular arc aerofoils as shown in Figure 3(a); the thickness-to-chord ratio is equal to 0·2 and the pitch-to-chord ratio is equal to 2·0. In Figure 3(b) the applied 60 × 30 grid is shown formed in the lower half of the symmetric blade-to-blade passage. The imposed boundary conditions are as follows.

(i) For the inlet section AB:

$$u = \text{constant}, \qquad w = 0, \qquad \partial p/\partial x = 0.$$

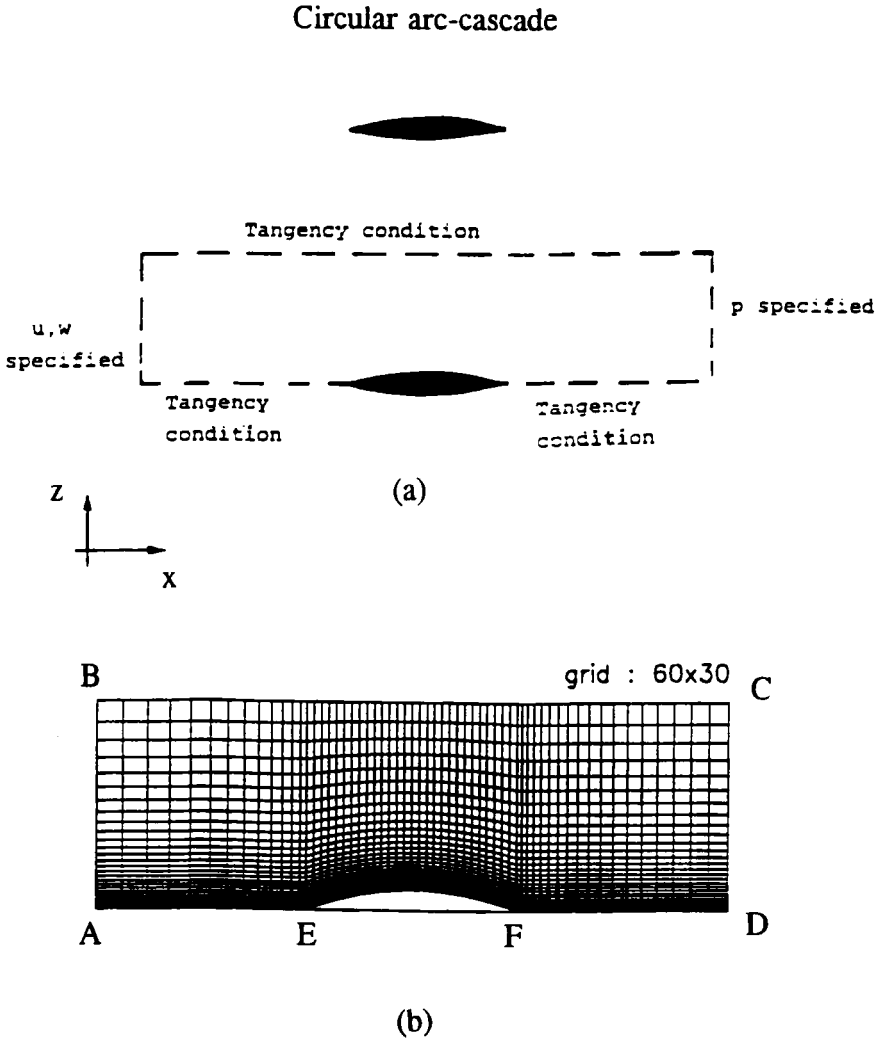

Figure 3. Geometry of circular arc cascade with boundary conditions and grid

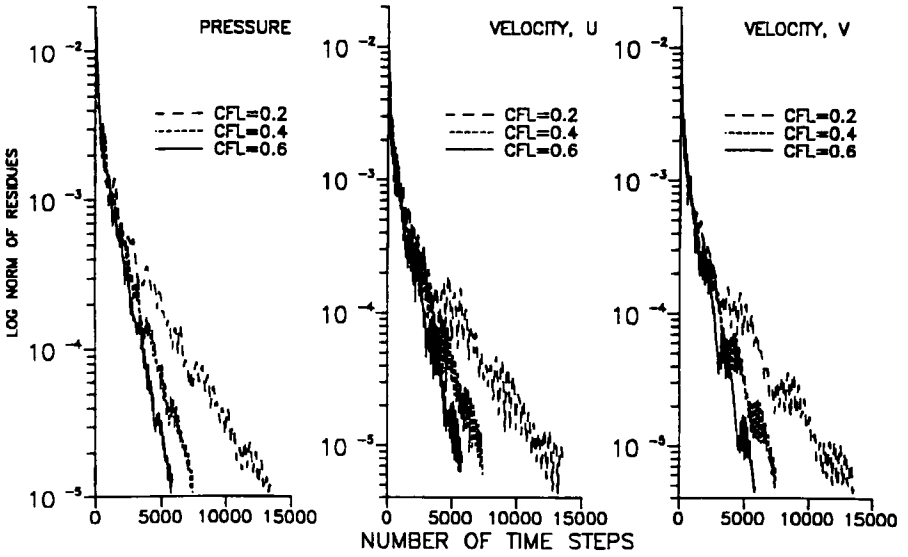

Figure 4. Effect of CFL on convergence history for $Re = 100$

(ii) For the outlet section CD:

$$\partial u/\partial x = 0, \qquad \partial w/\partial x = 0, \qquad p = \text{prescribed}.$$

(iii) For the upper limit BC (plane of symmetry):

$$\partial u/\partial z = 0, \qquad w = 0, \qquad \partial p/\partial z = 0.$$

(iv) For the lower limit AEFD:

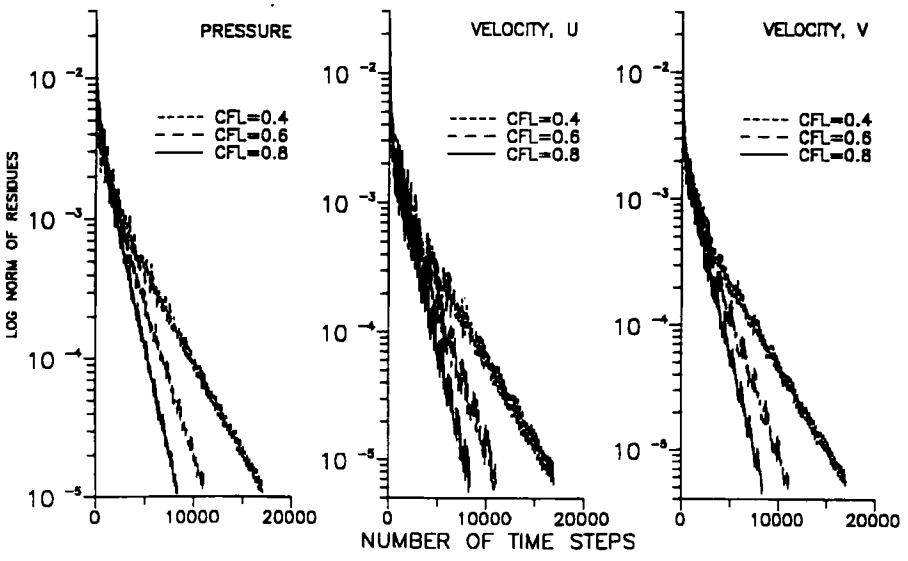

Figure 5. Effect of CFL on convergence history for $Re = 1000$

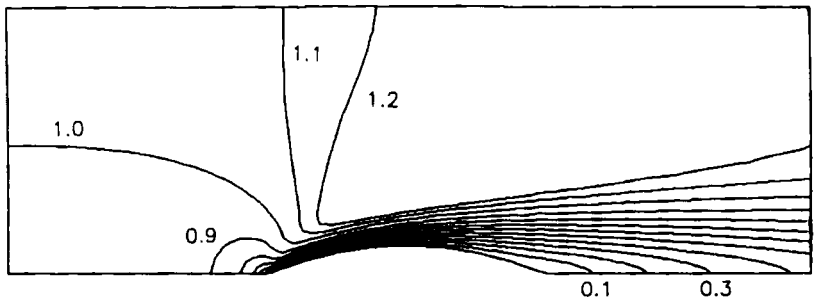

Figure 6. Velocity contours for cascade flow at $Re = 100$

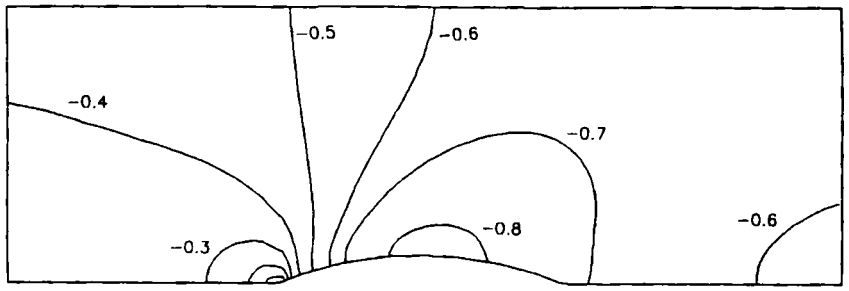

Figure 7. Pressure coefficient contours for cascade flow at $Re = 100$

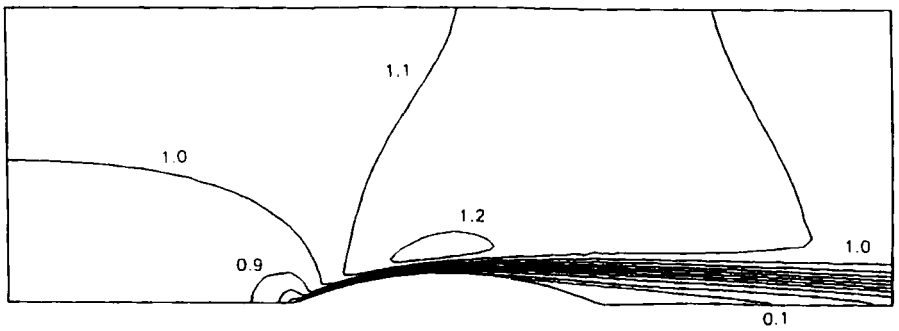

Figure 8. Velocity contours for cascade flow at $Re = 1000$

(a) on the sections AE and FD (plane of symmetry)

$$\partial u/\partial z = 0, \qquad w = 0, \qquad \partial p/\partial z = 0;$$

(b) on the aerofoil section EF

$$u = 0, \qquad w = 0, \qquad p \text{ defined by characteristic values } p_1 \text{ and } p_2.$$

For the third-order upwind differencing schemes fictitious cells on the solid surface are considered. The values in these cells are estimated by extrapolation of the values in the inner flow field.

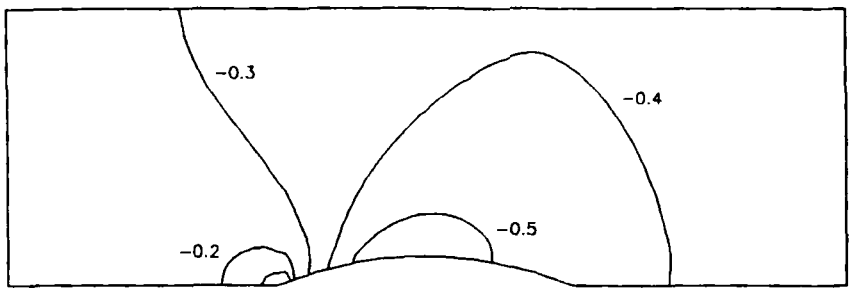

Figure 9. Pressure coefficient contours for cascade flow at $Re = 1000$

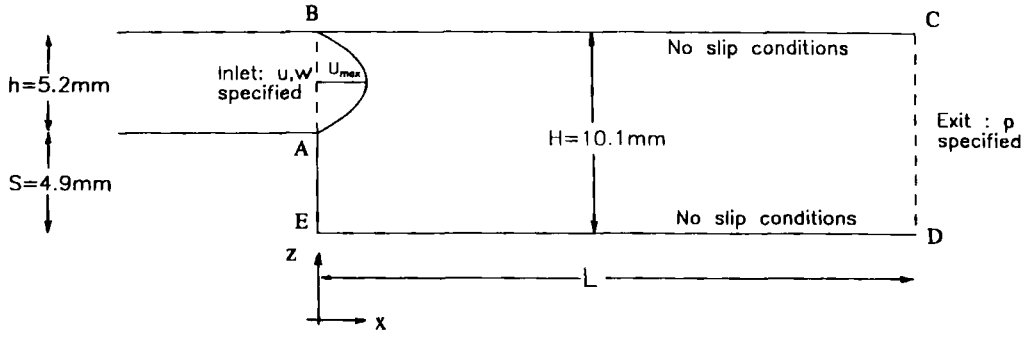

Figure 10. Backward-facing step geometry with channel dimensions and boundary conditions

In all cases convergence is considered to be attained when the normalized residual of all quantities becomes less than 1×10^{-5}. The numerical method is applied to two values of the Reynolds number, $Re = 100$ and 1000 ($Re = uD/\nu$, where u is the velocity at the inlet section AB, ν is the kinematic viscosity of the fluid and D is half the chord ratio), and for several values of the parameter β of artificial compressibility. It is proved that the best convergence rate is obtained with $\beta = 1$.

The effect of the CFL-value on the convergence rate is shown in Figures 4 and 5 for $Re = 100$ and 1000 respectively. From these figures it is evident that the fastest convergence is achieved with $CFL = 0{\cdot}6$ and $0{\cdot}8$ for $Re = 100$ and 1000 respectively.

In Figures 6 and 7 the obtained normalized pressure (taking as reference the stagnation pressure at the leading edge) and iso-velocity contours are shown for $Re = 100$. In Figures 8 and 9 the same results are shown for $Re = 1000$.

5.2. *Flow over a backward-facing step*

Validation of the method was obtained by comparing with experimental results for the flow over a backward-facing step. The configuration of the backward-facing step is shown in Figure 10. The applied boundary conditions are as follows.

(i) Inlet section AB at $x = 0$:

$$u \text{ measured profile}, \qquad w = 0, \qquad \partial p/\partial x = 0.$$

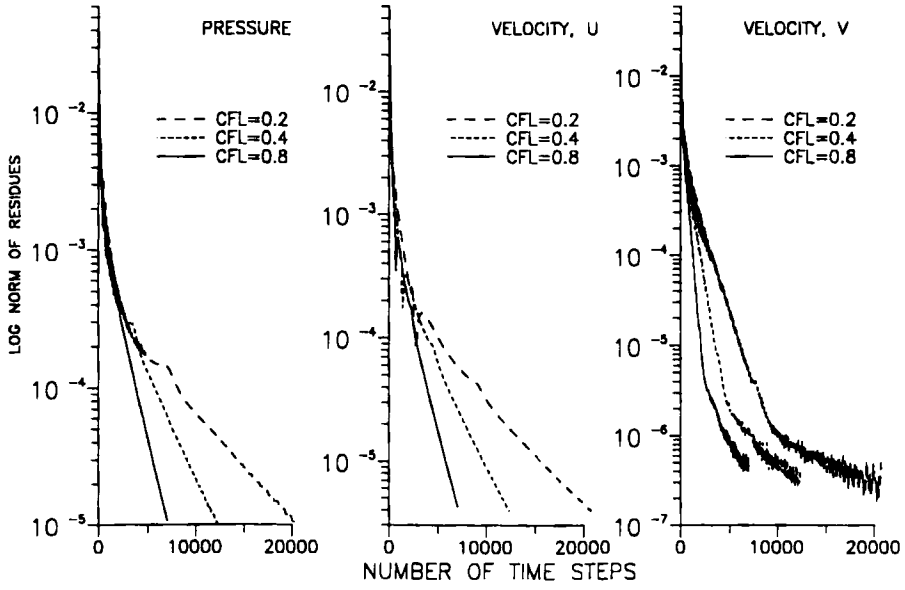

Figure 11. Effect of *CFL* on convergence history for $Re = 100$ and 75×20 grid

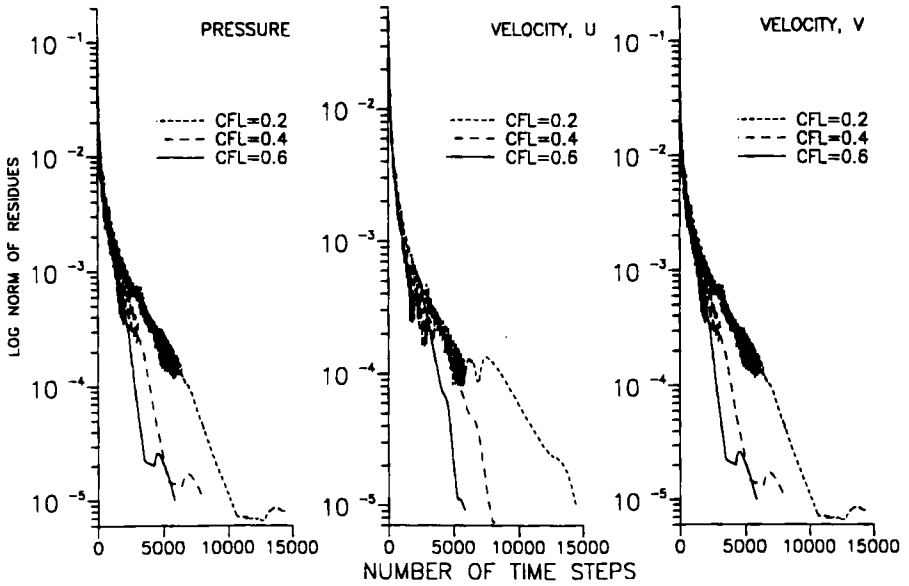

Figure 12. Effect of *CFL* on convergence history for $Re = 389$ and 75×20 grid

(ii) Outlet section CD at $x = L = 60S$:

$$\partial u/\partial x = 0, \qquad \partial w/\partial x = 0, \qquad p \text{ prescribed.}$$

(iii) Solid surfaces:

(a) sections ED and BC

$$u = 0, \qquad w = 0, \qquad p \text{ defined by characteristic values } p_1 \text{ and } p_2;$$

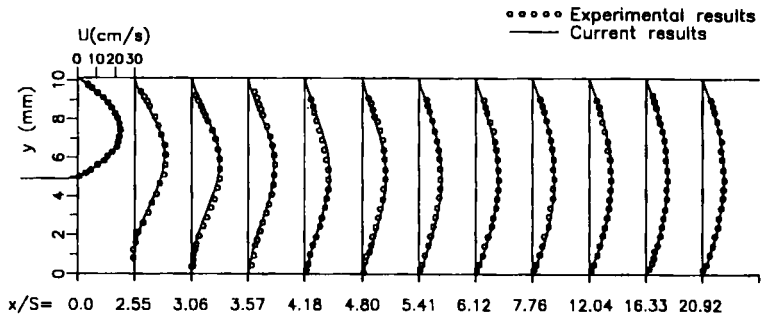

Figure 13. Present computed and experimental velocity profiles for $Re = 100$, $CFL = 0{\cdot}8$ and 75×20 grid at different x/S locations

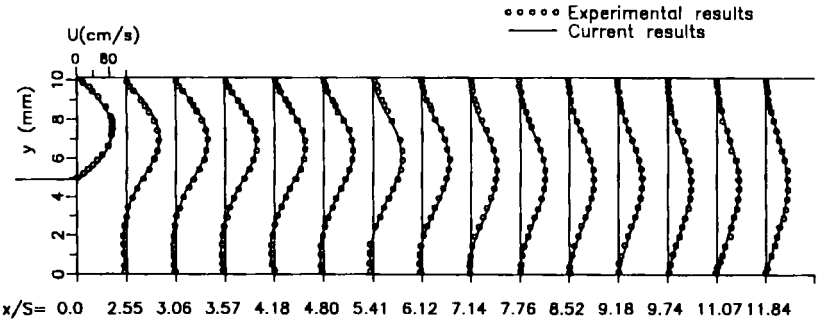

Figure 14. Present computed and experimental velocity profiles for $Re = 389$, $CFL = 0{\cdot}6$ and 75×20 grid at different x/S locations

(b) section AE

$$u = 0, \qquad w = 0, \qquad p \text{ as above.}$$

The obtained numerical results are compared with measurements in the case of $Re = 100$ and 389. Here the Reynolds number is defined as $Re = VD/\nu$, where V is equal to two-thirds of the measured maximum velocity at the inlet section AB, D is the hydraulic diameter of the inlet ($D = 2h$) and ν is the kinematic viscosity of the fluid.

The convergence histories for various CFL-values for $Re = 100$ and 389 are shown in Figures 11 and 12 respectively. For these cases a grid of 75×20 was used. As in the previous case, the convergence becomes faster as CFL increases. By additional calculations it has been proved that the best convergence rate is obtained with $\beta = 1$.

In Figures 13 and 14 the u-velocity profiles are compared with the measured ones for $Re = 100$ and 389 respectively. The comparison is very good in all sections for both cases ($Re = 100$ and 389).

The dependence of the obtained numerical results on the grid density has also been studied. The convergence histories for $CFL = 0{\cdot}60$, $\beta = 1$, $Re = 389$ and three different grids are shown in Figure 15. As expected, the convergence becomes faster as the grid becomes coarser. As far as the u-velocity profiles are concerned, it can be observed from Figure 16 that the numerical results obtained with the 75×20 and 150×40 grids are identical and therefore in excellent

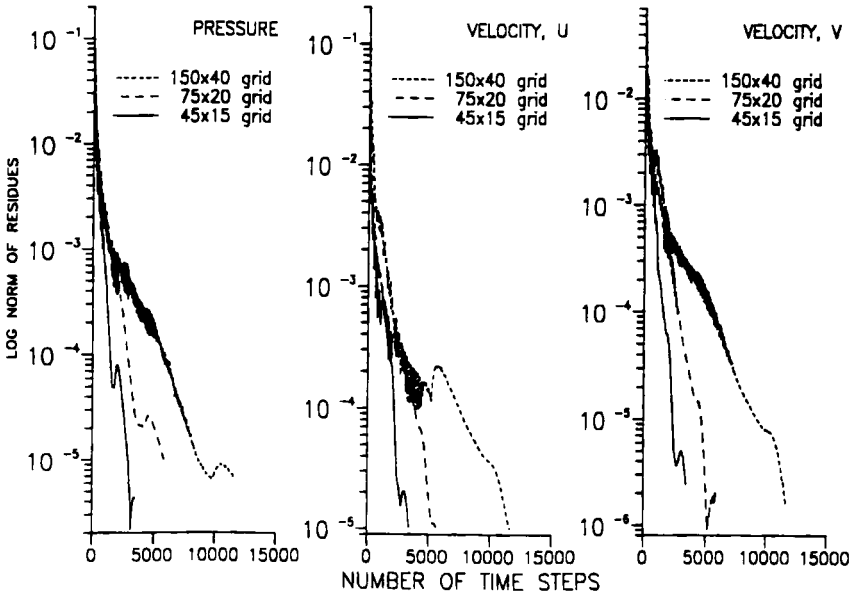

Figure 15. Effect of grid size on convergence history for $Re = 389$ and CFL $= 0{\cdot}6$

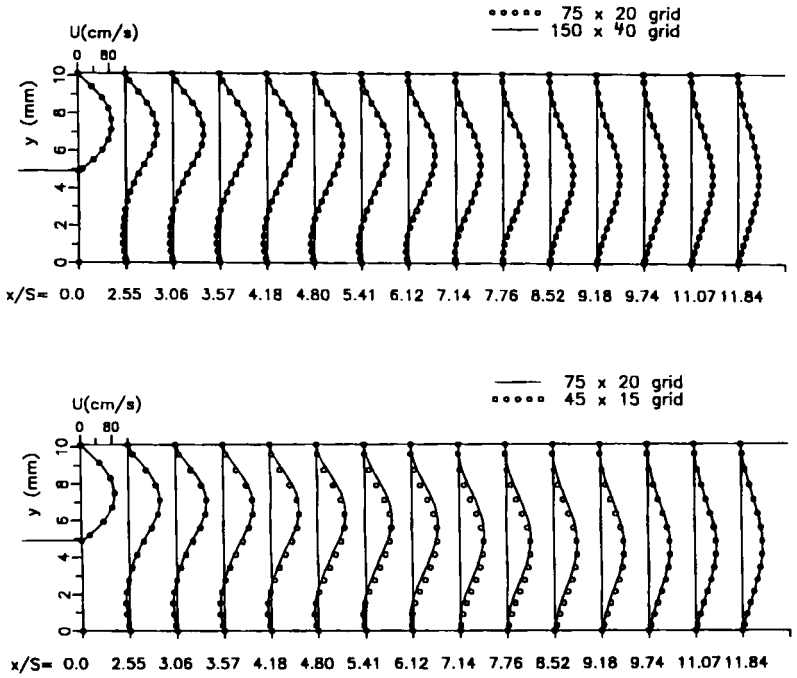

Figure 16. Effect of grid size on computed results for $Re = 389$ and $CFL = 0{\cdot}6$

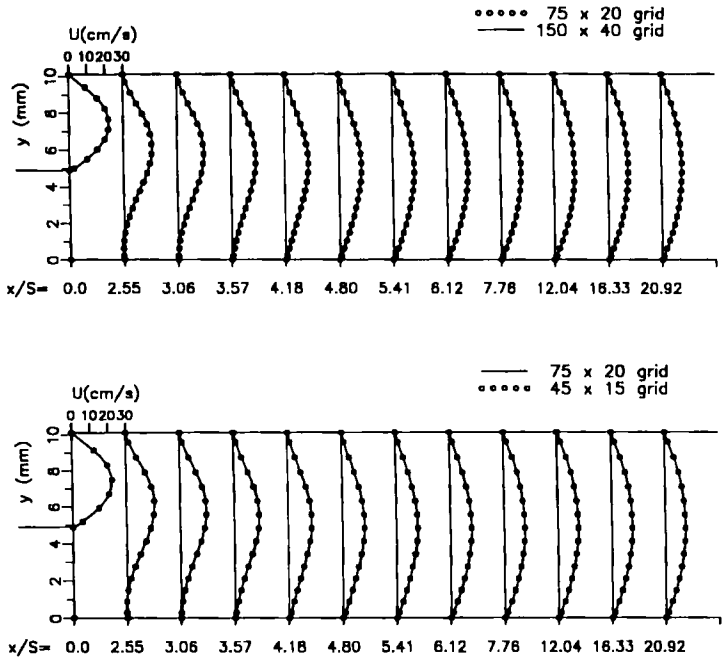

Figure 17. Effect of grid size on computed results for $Re = 100$ and $CFL = 0{\cdot}8$

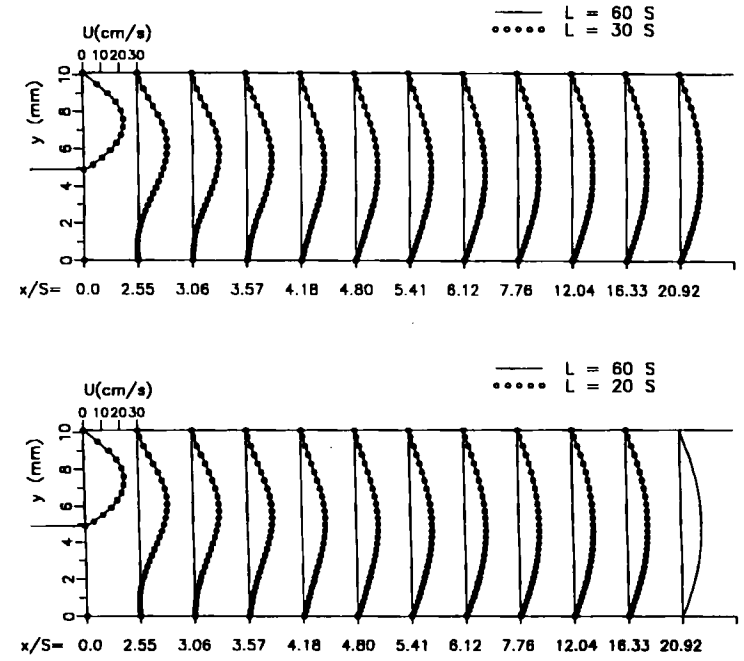

Figure 18. Effect of downstream boundary location on computed results for $Re = 100$ and $CFL = 0{\cdot}8$

Table I. Numbers of iterations for different grids

Grid	$Re = 100$	$Re = 389$
45 × 15	3920	3440
75 × 20	7040	5820
150 × 40	11640	19720

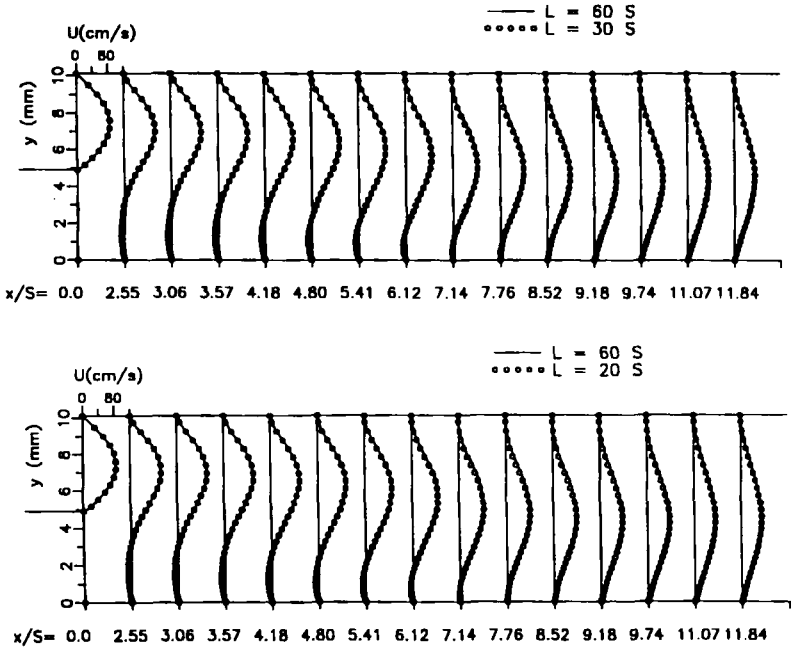

Figure 19. Effect of downstream boundary location on computed results for $Re = 389$ and $CFL = 0{\cdot}6$

agreement with the measured profiles. The results obtained with the coarse grid of 45 × 15 points exhibit small deviations from the measured values. In the case of $Re = 100$ (Figure 17) the numerical results are identical for the three different grids examined. The numbers of iterations for each case are given in Table I.

The effect of the distance L between the inlet and the outlet section (Figure 10) on the obtained results is also examined. In Figures 18 and 19 for $Re = 100$ and 389 respectively the u-velocity profiles are shown for three different values of L, namely $L = 20S$, $30S$ and $60S$. In all cases the effect of the distance L on the obtained results is negligible.

Finally, it should be mentioned that a mesh-sequencing scheme[19] was used for the case of the backward-facing step and $Re = 389$. Using three successive grids (20 × 6, 39 × 11, 77 × 21), a reduction of 48% in the run time was reached in comparison with the run time without the application of the mesh-sequencing scheme.

6. CONCLUSIONS

The objective of the present work was to develop a new numerical method for the solution of the incompressible Navier–Stokes equations. This method is used for the discretization of the convective fluxes of the Navier–Stokes equations and is based on a characteristic flux averaging of the inviscid fluxes according to the sign of the local eigenvalue. The present characteristic method is the extension to incompressible flows of a local Riemann solver presented in the past for the solution of inviscid and viscous compressible equations. The formulation of the method was examined and validation was presented for different flow cases, comparing also with experimental results.

Using the artificial compressibility formulation, a hyperbolic set of equations for the inviscid incompressible case is derived. By exploiting the hyperbolic properties of this system of equations, simple formulae for the definition of the primitive variables at the cell face of the computational volume can be derived. These formulae define the primitive variables as functions of their corresponding values on the characteristics. The computational results proved that the characteristic-based method provides high accuracy. For the time integration an explicit Runge–Kutta scheme was used. The numerical scheme is stable for the flow cases studied here and allows the use of CFL-values up to 0·8. A reduction of the number of iterations is expected from an implicit formulation of the characteristic-based method. Extension of the method to turbulent flows will also be a subject of future research.

REFERENCES

1. F. H. Harlow and J. E. Welch, 'Numerical calculation of time dependent viscous incompressible flow with free surface', *Phys. Fluids*, **8**, 2182–2189 (1965).
2. G. D., Raithby and G. E. Schneider, 'Numerical solution of problems in incompressible fluid flow: treatment of the velocity–pressure coupling', *Numer. Heat Transfer*, **2**, 417–440 (1979).
3. S. V. Patankar, *Numerical Heat Transfer and Fluid Flow*, Hemisphere, New York, 1980.
4. A. J. Chorin, 'A numerical method for solving incompressible viscous flow problems', *J. Comput. Phys.*, **2**, 12–26 (1967).
3. J. L. Steger and P. Kutler, Implicit finite difference procedures for the computation of vortex wakes', *AIAA J.*, **15**, 581–590 (1977).
6. R. Peyret and T. D. Taylor, *Computational Methods for Fluid Flow*, Springer, New York, 1983.
7. A. Rizzi and L. Erikson, 'Computation of inviscid incompressible flow with rotation', *J. Fluid Mech.*, **153**, 275–312 (1985).
8. D. Choi and C. L. Merkle, 'Application of time-iterative schemes to incompressible flow', *AAIA J.*, **23**, 1519–1524 (1985).
9. D. Kwak, J. L. C. Chang, S. P. Shanks and S. R. Chakravarthy, 'A three dimensional incompressible flow solver using primitive variables', *AIAA J.*, **24**, 390–396 (1986).
10. C. Merckle and M. A. Athavale, 'Time accurate unsteady incompressible flow algorithms based on artificial compressibility', *AIAA Paper 87-1137*, 1987.
11. P.-M. Hartwich, C.-H. Hsu and C. H. Liu, 'Vectorizable implicit algorithms for the flux-difference split, three dimensional Navier–Stokes equations', *J. Fluids Eng.*, **110**, 297–305 (1988).
12. S. E. Rogers and D. Kwak, 'An upwind differencing scheme for the steady state incompressible Navier–Stokes equations, *NASA TM 101051*, 1988.
13. S. E. Rogers and D. Kwak, 'Upwind differencing scheme for the time accurate incompressible Navier–Stokes equations', *AIAA J.*, **28**, 253–262 (1990).
14. E. Dick and J. Linden, 'A multigrid method for steady incompressible Navier–Stokes equations based on flux difference splitting', *Int. J. numer. methods fluids*, **14**, 1311–1323 (1992).
15. V. Michelassi and C. Benocci, 'Prediction of incompressible flow separation with the approximate factorization technique', *Int. J. numer. methods fluids*, **7**, 1383–1403 (1987).
16. C. A. J. Fletcher, *Computational Techniques for Fluid Dynamics*, Vol. II, Springer, New York, 1983.
17. J. D. Ramshaw and G. L. Mesina, 'A hybrid penalty–pseudocompressibility method for transient incompressible fluid flow', *Comput. Fluids*, **20**, 165–175 (1991).
18. A. Eberle, '3d Euler calculations using characteristic flux extrapolation', *AIAA Paper 85-0119*, 1985.
19. D. Drikakis, 'Development of upwind numerical methods in high speed aerodynamics', *Ph.D. Thesis*, National Technical University of Athens, 1993.

20. D. Drikakis and S. Tsangaris, 'An implicit characteristic flux averaging scheme for the Euler equations for real gases,' *Int. J. numer. methods fluids*, **12**, 771–726 (1991).
21. D. Drikakis and S. Tsangaris, 'On the solution of the compressible Navier–Stokes equations using improved flux vector splitting methods', *Appl. Math. Modell.*, **17**, 282–297 (1993).
22. A. Jameson, W. Schmidt and T. Turkel, 'Numerical solutions of the Euler equations by finite volume methods using Runge–Kutta time-stepping schemes', *AIAA Paper 81-1259*, 1981.
23. C. Hirsch, *Numerical Computation of Internal and External Flows*, Vol. I, Wiley, Chichester, 1988.
24. A. Eberle, 'Characteristic flux averaging approach to the solution of Euler's equations', *VKI Lecture Ser. 1987-04*, 1987.
25. R. Courant and D. Hilbert, *Methoden der Mathematischen Physik I*, Springer, Berlin, 1968.
26. S. R. Chakravarthy, 'High resolution upwind formulations for the Navier–Stokes equations', *VKI Lecture Ser. 1988-05*, 1988.
27. M. L. Mansour and A. Hamed, 'Implicit solution of the incompressible Navier–Stokes equations in primitive variables', *AAIA Paper 88-0717*, 1988.
28. M. L. Mansour and A. Hamed, 'Implicit solution of the incompressible Navier–Stokes equations on a non-staggered grid', *J Comput. Phys.*, **86**, 147–167 (1990).
29. B. F. Armaly, F. Durst, J. C. F. Pereira and B. Schonung, 'Experimental and theoretical investigation of backward-facing step flow', *J. Fluid Mech.*, **127**, 473–496 (1983).